

# Thiophosphate Phase Diagrams Developed in Conjunction with the Synthesis of the New Compounds $\text{KLaP}_2\text{S}_6$ , $\text{K}_2\text{La}(\text{P}_2\text{S}_6)_{1/2}(\text{PS}_4)$ , $\text{K}_3\text{La}(\text{PS}_4)_2$ , $\text{K}_4\text{La}_{0.67}(\text{PS}_4)_2$ , $\text{K}_{9-x}\text{La}_{1+x/3}(\text{PS}_4)_4$ ( $x = 0.5$ ), $\text{K}_4\text{Eu}(\text{PS}_4)_2$ , and $\text{KEuPS}_4$

Carl R. Evenson IV and Peter K. Dorhout\*,†

Department of Chemistry, Colorado State University, Fort Collins, Colorado 80523

Received June 2, 2000

An alkali-metal sulfur reactive flux has been used to synthesize a series of quaternary rare-earth metal compounds. These include  $\text{KLaP}_2\text{S}_6$  (**I**),  $\text{K}_2\text{La}(\text{P}_2\text{S}_6)_{1/2}(\text{PS}_4)$  (**II**),  $\text{K}_3\text{La}(\text{PS}_4)_2$  (**III**),  $\text{K}_4\text{La}_{0.67}(\text{PS}_4)_2$  (**IV**),  $\text{K}_{9-x}\text{La}_{1+x/3}(\text{PS}_4)_4$  ( $x = 0.5$ ) (**V**),  $\text{K}_4\text{Eu}(\text{PS}_4)_2$  (**VI**), and  $\text{KEuPS}_4$  (**VII**). Compound **I** crystallizes in the monoclinic space group  $P2_1/c$  with the cell parameters  $a = 11.963(12)$  Å,  $b = 7.525(10)$  Å,  $c = 11.389(14)$  Å,  $\beta = 109.88(4)^\circ$ , and  $Z = 4$ . Compound **II** crystallizes in the monoclinic space group  $P2_1/n$  with  $a = 9.066(6)$  Å,  $b = 6.793(3)$  Å,  $c = 20.112(7)$  Å,  $\beta = 97.54(3)^\circ$ , and  $Z = 4$ . Compound **III** crystallizes in the monoclinic space group  $P2_1/c$  with  $a = 9.141(2)$  Å,  $b = 17.056(4)$  Å,  $c = 9.470(2)$  Å,  $\beta = 90.29(2)^\circ$ , and  $Z = 4$ . Compound **IV** crystallizes in the orthorhombic space group  $Ibam$  with  $a = 18.202(2)$  Å,  $b = 8.7596(7)$  Å,  $c = 9.7699(8)$  Å, and  $Z = 4$ . Compound **V** crystallizes in the orthorhombic space group  $Ccca$  with  $a = 17.529(9)$  Å,  $b = 36.43(3)$  Å,  $c = 9.782(4)$  Å, and  $Z = 8$ . Compound **VI** crystallizes in the orthorhombic space group  $Ibam$  with  $a = 18.29(5)$  Å,  $b = 8.81(2)$  Å,  $c = 9.741(10)$  Å, and  $Z = 4$ . Compound **VII** crystallizes in the orthorhombic space group  $Pnma$  with  $a = 16.782(2)$  Å,  $b = 6.6141(6)$  Å,  $c = 6.5142(6)$  Å, and  $Z = 4$ . The sulfur compounds are in most cases isostructural to their selenium counterparts. By controlling experimental conditions, these structures can be placed in quasi-quaternary phase diagrams, which show the reaction conditions necessary to obtain a particular thiophosphate anionic unit in the crystalline product. These structures have been characterized by Raman and IR spectroscopy and UV–vis diffuse reflectance optical band gap analysis.

## Introduction

The reactive flux method continues to be an active research tool for the synthesis of new chalcogenide materials with interesting optical, magnetic, and semiconducting properties. While many new compounds with transition,<sup>1–3</sup> main-group,<sup>4,5</sup> and rare-earth (RE) metals<sup>6–11</sup> have been reported, there have been few attempts to understand how the reactive flux technique can be manipulated to produce predictable compounds with desirable properties. In the preceding paper in this issue, we described a detailed, rational approach to the solid-state synthesis of new quaternary rare-earth-metal selenophosphate structures

using the reactive flux method.<sup>12</sup> By comparing reactions isometric in selenium, a series of quaternary reactions yielding different products could be plotted on a ternary phase diagram. In this paper we describe the extension of this concept to thiophosphate chemistry.

## Experimental Section

**Synthesis.** Crystals of all compounds observed were obtained using the same procedure. The following reactants were used as received and stored in an inert atmosphere glovebox: La (99.999%, Ames Laboratory), Eu (99.95%, Ames Laboratory), P (Mallinckrodt Red), S (99.999%, Johnson-Matthey).  $\text{K}_2\text{S}_2$  was previously made in liquid ammonia from the stoichiometric combination of the elements.<sup>13,14</sup> Reactants were loaded into fused silica ampules inside an inert atmosphere glovebox. Each ampule was flame sealed under vacuum and placed in a temperature-controlled tube furnace. The furnace was ramped to 725 °C, where it remained for 150 h. The furnace was then allowed to cool back to room temperature at 4 °C/h. Crystals were separated from excess flux by washing the reaction product with dimethylformamide (DMF).

$\text{KLaP}_2\text{S}_6$  (**I**) was synthesized by combining 58.2 mg (1.82 mmol) of S, 28.7 mg (0.202 mmol) of  $\text{K}_2\text{S}_2$ , 43.7 mg (1.411 mmol) of P, and 28.0 mg (0.202 mmol) of La. The reaction yielded clear colorless crystals.

$\text{K}_2\text{La}(\text{P}_2\text{S}_6)_{1/2}(\text{PS}_4)$  (**II**) was synthesized by combining 36.7 mg (1.13 mmol) of S, 45.9 mg (0.322 mmol) of  $\text{K}_2\text{S}_2$ , 20.0 mg (0.646 mmol) of P, and 22.4 mg (0.161 mmol) of La. The reaction yielded clear colorless crystals.

\* To whom correspondence should be addressed: E-mail: pkd@LAMAR.colostate.edu.

- † P.K.D. is a Camille Dreyfus Teacher Scholar and an A. P. Sloan Fellow.
- (1) Dorhout, P. K.; Malo, T. M. *Z. Anorg. Allg. Chem.* **1996**, *622*, 385–391.
  - (2) Tremel, W.; Kleinke, H.; Derstroff, V.; Reisner, C. *J. Alloys Compd.* **1995**, *219*, 73–82.
  - (3) Chondroudis, K.; Kanatzidis, M. G. *J. Solid State Chem.* **1998**, *138*, 321–328.
  - (4) Chondroudis, K.; Kanatzidis, M. G. *J. Solid State Chem.* **1998**, *136*, 79–86.
  - (5) McCarthy, T. J.; Kanatzidis, M. G. *J. Chem. Soc., Chem. Commun.* **1994**, 1089.
  - (6) Chen, J. H.; Dorhout, P. K. *Inorg. Chem.* **1995**, *34*, 5705–5706.
  - (7) Chen, J. H.; Dorhout, P. K.; Ostenson, J. E. *Inorg. Chem.* **1996**, *35*, 5627–5633.
  - (8) Chen, J. H.; Dorhout, P. K. *J. Alloys Compd.* **1997**, *249*, 199–205.
  - (9) Gauthier, G.; Jobic, S.; Brec, R.; Rouxel, J. *Inorg. Chem.* **1998**, *37*, 2332–2333.
  - (10) Gauthier, G.; Jobic, S.; Boucher, F.; Macaudiere, P.; Huguénin, D.; Rouxel, J.; Brec, R. *Chem. Mater.* **1998**, *10*, 2341–2347.
  - (11) Chondroudis, K.; Kanatzidis, M. G. *Inorg. Chem.* **1998**, *37*, 3792–3797.

(12) Evenson, C. R.; Dorhout, P. K. *Inorg. Chem.* **2001**, *40*, 2875–2883.

(13) Liao, J.-H.; Kanatzidis, M. G. *Inorg. Chem.* **1992**, *31*, 431–439.

(14) Schewe-Miller, I. *Metallreiche Hauptgruppenmetall-Chalkogenverbindungen: Synthese, Strukturen und Eigenschaften*; Max-Planck-Institut für Festkörperforschung: Stuttgart, Germany, 1990.

**Table 1.** Crystallographic Data for  $\text{KLaP}_2\text{S}_6$ ,  $\text{K}_2\text{La}(\text{P}_2\text{S}_6)_{1/2}(\text{PS}_4)$ ,  $\text{K}_3\text{La}(\text{PS}_4)_2$ ,  $\text{K}_4\text{La}_{0.67}(\text{PS}_4)_2$ ,  $\text{K}_{9-x}\text{La}_{1+x/3}(\text{PS}_4)_4$  ( $x = 0.5$ ),  $\text{K}_4\text{Eu}(\text{PS}_4)_2$ , and  $\text{KEuPS}_4$ 

	$\text{KLaP}_2\text{S}_6$ (I)	$\text{K}_2\text{LaP}_2\text{S}_7$ (II)	$\text{K}_3\text{La}(\text{PS}_4)_2$ (III)	$\text{K}_4\text{La}_{0.67}(\text{PS}_4)_2$ (IV)	$\text{K}_{9-x}\text{La}_{1+x/3}(\text{PS}_4)_4$ (V)	$\text{K}_4\text{Eu}(\text{PS}_4)_2$ (VI)	$\text{KEuPS}_4$ (VII)
fw	432.31	503.47	574.63	567.89	1131.02	626.78	350.27
$a$ , Å	11.963(12)	9.066(6)	9.141(2)	18.202(2)	17.529(9)	18.29(5)	16.782(2)
$b$ , Å	7.525(10)	6.793(3)	17.056(4)	8.7596(7)	36.43(3)	8.81(2)	6.6141(6)
$c$ , Å	11.389(14)	20.112(7)	9.470(2)	9.7699(8)	9.782(4)	9.741(10)	6.5142(6)
$\alpha$ , deg	90.0	90.0	90.0	90.0	90.0	90.0	90.0
$\beta$ , deg	109.88(4)	97.54(3)	90.29(2)	90.0	90.0	90.0	90.0
$\gamma$ , deg	90.0	90.0	90.0	90.0	90.0	90.0	90.0
$V$ , Å <sup>3</sup>	964(2)	1227.9(10)	1476.5(6)	1557.7(2)	6246(6)	1570(5)	723.04(11)
$Z$	4	4	4	4	8	4	4
$\lambda(\text{Mo K}\alpha)$ , Å	0.71073	0.71073	0.71073	0.71073	0.71073	0.71073	0.71073
space group	$P2_1/c$ (no. 14)	$P2_1/n$ (no. 14)	$P2_1/c$ (no. 14)	$Ibam$ (no. 72)	$Ccca$ (no. 68)	$Ibam$ (no. 72)	$Pnma$ (no. 62)
temp, K	169(2)	169(2)	168(2)	170(2)	167(2)	168(2)	168(2)
$\rho_{\text{calcd}}$ , Mg/m <sup>3</sup>	2.978	2.724	2.585	2.421	2.405	2.651	3.218
$\mu$ , mm <sup>-1</sup>	6.415	5.552	5.046	4.171	3.995	6.285	10.504
$R1$ , %	5.83	4.93	3.86	4.69	6.76	4.95	3.68
$wR2$ , %	11.20	7.65	7.66	10.43	11.60	10.55	6.87

$$^a R1 = \sum(|F_o| - |F_c|) / \sum |F_o|. \quad wR2 = [\sum [w(F_o^2 - F_c^2)^2] / \sum [w(F_o^2)^2]]^{1/2}.$$

$\text{K}_3\text{La}(\text{PS}_4)_2$  (III) was synthesized by combining 37.0 mg (1.15 mmol) of S, 46.9 mg (0.330 mmol) of  $\text{K}_2\text{S}_2$ , 10.2 mg (0.330 mmol) of P, and 22.9 mg (0.165 mmol) of La. Clear colorless crystals were found in the reaction product.

$\text{K}_4\text{La}_{0.67}(\text{PS}_4)_2$  (IV) was synthesized by combining 22.1 mg (0.689 mmol) of S, 28.0 mg (0.197 mmol) of  $\text{K}_2\text{S}_2$ , 6.10 mg (0.197 mmol) of P, and 27.4 mg (0.197 mmol) of La. Clear colorless crystals were found in the reaction product.

$\text{K}_{9-x}\text{La}_{1+x/3}(\text{PS}_4)_4$  ( $x = 0.5$ ) (V) was synthesized by combining 42.2 mg (1.32 mmol) of S, 53.5 mg (0.375 mmol) of  $\text{K}_2\text{S}_2$ , 11.6 mg (0.375 mmol) of P, and 26.1 mg (0.188 mmol) of La. The reactants were placed in a fused silica ampule, sealed under vacuum, and placed in a tube furnace. The tube furnace was held at 525 °C for 150 h and allowed to cool at 4 °C/h. Clear colorless crystals were separated from excess flux. The equivalent reaction at 725 °C yielded crystals of  $\text{K}_3\text{La}(\text{PS}_4)_2$  instead of  $\text{K}_{9-x}\text{La}_{1+x/3}(\text{PS}_4)_4$  ( $x = 0.5$ ).

$\text{K}_4\text{Eu}(\text{PS}_4)_2$  (VI) was synthesized by combining 44.0 mg (1.37 mmol) of S, 55.8 mg (0.392 mmol) of  $\text{K}_2\text{S}_2$ , 12.1 mg (0.392 mmol) of P, and 29.8 mg (0.196 mmol) of Eu. The reaction yielded a binary product composed of clear colorless  $\text{K}_3\text{PS}_4$  crystals and dark brown  $\text{K}_4\text{Eu}(\text{PS}_4)_2$  crystals.

$\text{KEuPS}_4$  (VII) was synthesized by combining 50.7 mg (1.58 mmol) of S, 25.0 mg (0.176 mmol) of  $\text{K}_2\text{S}_2$ , 10.9 mg (0.352 mmol) of P, and 26.7 mg (0.176 mmol) of Eu in an inert atmosphere drybox. The reactants were placed in a fused silica ampule, sealed under vacuum, and placed in a tube furnace. The tube furnace was held at 525 °C for 150 h and allowed to cool at 4 °C/h. The reaction product yielded clear light brown plates of  $\text{KEuPS}_4$ . A second reaction with the same stoichiometry showed that  $\text{KEuPS}_4$  could also be synthesized at 725 °C.

**Physical Measurements. Single-Crystal X-ray Diffraction.** Intensity data sets for crystals I–VII were collected using a Bruker Smart CCD diffractometer. Each intensity data set was integrated using SAINT,<sup>15</sup> a SADABS absorption correction was applied,<sup>16</sup> and the structure was solved by direct methods using SHELXTL.<sup>17</sup> Crystallographic data for compounds I–VII are reported in Table 1.

**Raman Spectroscopy.** The solid-state Raman spectra of compounds I, II, VI, and VII were taken with a Nicolet Magna-IR 760 spectrometer with a FT-Raman module attachment using a Nd:YAG excitation laser (1064 nm).

**IR Spectroscopy.** The IR spectrum of compound I was taken on a Nicolet Magna-IR 760 spectrometer as a KBr pellet with a pure KBr pellet subtracted with the background.

**UV–Vis Spectroscopy.** Diffuse reflectance measurements were taken with a Varian Cary 500 Scan UV–vis–near-IR spectrophotometer equipped with a Praying Mantis accessory. A polytetrafluoroethylene standard was used as a reference. The Kubelka–Munk function was applied to obtain band gap information.<sup>18,19</sup>

## Results and Discussion

**Structures.** A single crystal of  $\text{KLaP}_2\text{S}_6$  (I) was selected, 6077 (2307 independent) reflections were collected, and an absorption correction was applied ( $R_{\text{int}} = 0.0929$ ). The structure was solved by direct methods in  $P2_1/c$  to electron density residuals of 1.563 and  $-1.677 \text{ e } \text{Å}^{-3}$ , and all atoms were refined anisotropically with SHELXTL using full-matrix least-squares refinement on  $F^2$  for 92 variables.<sup>17</sup>  $\text{KLaP}_2\text{S}_6$  is isostructural to  $\text{KLaP}_2\text{Se}_6$ .<sup>6</sup> It is a layered structure with each  ${}^2_{\infty}[\text{La}(\text{P}_2\text{S}_6)]^-$  layer separated by potassium cations. Within each layer lanthanum atoms are intricately linked together by  $(\text{P}_2\text{S}_6)^{4-}$  units. Each lanthanum atom is 9-coordinate with an average La–S bond distance of 3.08(1) Å. The nine sulfur atoms surrounding each lanthanum atom are part of four different  $(\text{P}_2\text{S}_6)^{4-}$  units. Figure 1 shows that each lanthanum is coordinated by two  $(\text{P}_2\text{S}_6)^{4-}$  units in a face-sharing manner, edge-sharing with a third  $(\text{P}_2\text{S}_6)^{4-}$  unit, and corner-sharing with a fourth  $(\text{P}_2\text{S}_6)^{4-}$  unit. The P–P bond length is 2.212(5) Å, and the average P–S bond length is 2.02(1) Å. Atomic coordinates and selected bond distances for  $\text{KLaP}_2\text{S}_6$  are reported in Tables 2 and 3, respectively.

A single crystal of  $\text{K}_2\text{La}(\text{P}_2\text{S}_6)_{1/2}(\text{PS}_4)$  or  $\text{K}_2\text{LaP}_2\text{S}_7$  (II) was selected, 7846 (2978 independent) reflections were collected, and an absorption correction was applied ( $R_{\text{int}} = 0.0796$ ). The structure was solved by direct methods in  $P2_1/n$  to electron density residuals of 1.353 and  $-1.214 \text{ e } \text{Å}^{-3}$ , and all atoms were refined anisotropically with SHELXTL using full-matrix least-squares refinement on  $F^2$  for 109 variables.<sup>17</sup>  $\text{K}_2\text{LaP}_2\text{S}_7$  is isostructural to  $\text{K}_2\text{LaP}_2\text{Se}_7$ .<sup>12</sup> It is a layered compound with  ${}^2_{\infty}[\text{La}(\text{P}_2\text{S}_6)_{1/2}(\text{PS}_4)]^{2-}$  layers lying in the (101) plane of the unit cell that are separated by potassium cations. Figure 2 shows that each layer is composed of lanthanum atoms coordinated by  $(\text{PS}_4)^{3-}$  tetrahedra and  $(\text{P}_2\text{S}_6)^{4-}$  ethane-like units. Within each layer, “chains” of lanthanum distorted square antiprisms coor-

(15) Data processing software for the SMART system; Bruker Analytical X-ray Instruments Inc.: Madison, WI, 1995.

(16) Sheldrick, G. M. SADABS; University of Gottingen: Gottingen, Germany, 1997.

(17) SHELXTL 5.03; Bruker Analytical X-ray Systems Inc.: Madison, WI, 1994.

(18) McCarthy, T. J.; Tanzer, T. A.; Kanatzidis, M. G. *J. Am. Chem. Soc.* **1995**, *117*, 1294–1301.

(19) Wilkinson, F.; Kelly, G. In *Diffuse Reflectance Flash Photolysis*; Scaiano, J. C., Ed.; CRC Press: Boca Raton, FL, 1989; Vol. 1, pp 293–314.

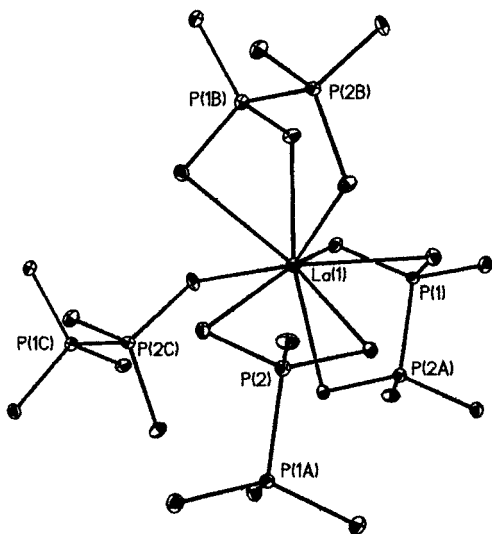


**Figure 1.** ORTEP plot of the lanthanum coordination environment in  $\text{KLaP}_2\text{S}_6$ . Thermal ellipsoids plotted at the 50% probability level. Potassium atoms left out for clarity.

**Table 2.** Fractional Atomic Coordinates and Equivalent Isotropic Displacement Parameters ( $\text{\AA}^2 \times 10^3$ )<sup>a</sup> for  $\text{KLaP}_2\text{S}_6$

	x	y	z	<i>U</i> (eq)
La(1)	0.6505(1)	0.1060(1)	0.9037(1)	9(1)
P(1)	0.7921(3)	0.1184(4)	1.2341(3)	8(1)
P(2)	0.3258(3)	0.1015(4)	0.7530(3)	9(1)
K(1)	1.1291(2)	0.0921(4)	1.3744(3)	15(1)
S(1)	0.6765(3)	0.1927(4)	0.6396(3)	11(1)
S(2)	0.4439(3)	-0.0152(4)	0.6828(3)	12(1)
S(3)	0.8875(3)	0.0233(4)	1.1341(3)	12(1)
S(4)	0.4090(3)	0.1867(4)	0.9311(3)	10(1)
S(5)	0.8738(3)	0.2968(4)	0.9104(3)	12(1)
S(6)	0.7801(3)	-0.2131(4)	0.8570(3)	12(1)

<sup>a</sup> *U*(eq) is defined as one-third of the trace of the orthogonalized  $U_{ij}$  tensor.

**Table 3.** Selected Bond Distances ( $\text{\AA}$ ) for  $\text{KLaP}_2\text{S}_6$

La(1)–S(6)	3.002(4)	P(1)–P(2)	2.212(5)
La(1)–S(2)	3.007(4)	P(1)–S(5)	2.016(5)
La(1)–S(4)	3.070(4)	P(1)–S(3)	1.998(5)
La(1)–S(4')	3.131(4)	P(1)–S(1)	2.019(5)
La(1)–S(3)	3.201(5)	P(2)–S(2)	2.044(5)
La(1)–S(1')	3.006(4)	P(2)–S(4)	2.035(5)
La(1)–S(5)	3.011(4)	P(2)–S(6)	2.010(5)
La(1)–S(2')	3.101(5)		
La(1)–S(1)	3.196(5)		

minated by  $(\text{PS}_4)^{3-}$  tetrahedra are linked into a layer with ethane-like  $(\text{P}_2\text{S}_6)^{4-}$  units. In this way each 8-coordinate lanthanum atom is edge-sharing with two  $(\text{PS}_4)^{3-}$  tetrahedra, corner-sharing with a third  $(\text{PS}_4)^{3-}$  tetrahedron, and bound in a sideways fashion to a  $(\text{P}_2\text{S}_6)^{4-}$  unit. The coordination environment of lanthanum in  $\text{K}_2\text{LaP}_2\text{S}_7$  is shown in Figure 3. Atomic coordinates and selected bond distances for  $\text{K}_2\text{LaP}_2\text{S}_7$  are reported in Tables 4 and 5, respectively.

A single crystal of  $\text{K}_3\text{La}(\text{PS}_4)_2$  or  $\text{K}_3\text{LaP}_2\text{S}_8$  (**III**) was selected, 9659 (3559 independent) reflections were collected, and an absorption correction was applied ( $R_{\text{int}} = 0.0499$ ). The structure was solved by direct methods in  $P2_1/c$  to electron density residuals of 1.197 and  $-1.974 \text{ e \AA}^{-3}$ , and all atoms were refined anisotropically with SHELXTL using full-matrix least-squares refinement on  $F^2$  for 127 variables.<sup>17</sup>  $\text{K}_3\text{LaP}_2\text{S}_8$  is isostructural to  $\text{K}_3\text{CeP}_2\text{S}_8$ <sup>9</sup> and  $\text{K}_3\text{LaP}_2\text{Se}_8$ .<sup>12</sup> The only difference between the sulfur and selenium versions of this structure is that, in the selenium case, lanthanum is 8-coordinate while the sulfur

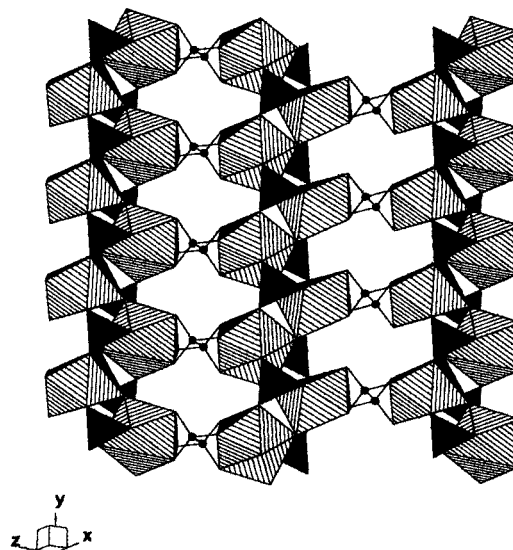


**Figure 2.**  $\text{K}_2\text{LaP}_2\text{S}_7$ : striped La–S polyhedra, black  $(\text{PS}_4)^{3-}$  tetrahedra, black phosphorus atoms in  $(\text{P}_2\text{S}_6)^{4-}$ . Potassium atoms left out for clarity.

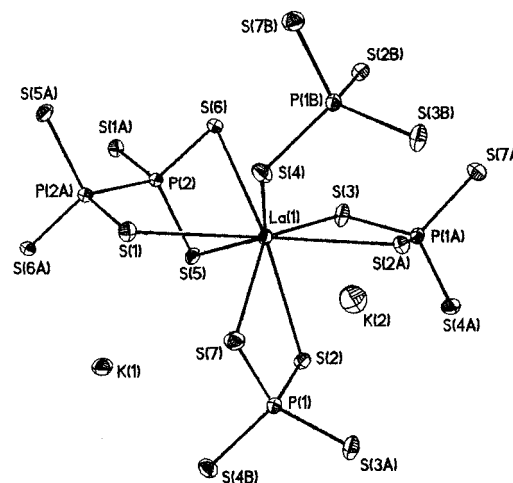


**Figure 3.** ORTEP plot of the lanthanum coordination environment in  $\text{K}_2\text{LaP}_2\text{S}_7$ . Thermal ellipsoids plotted at the 50% probability level.

**Table 4.** Fractional Atomic Coordinates and Equivalent Isotropic Displacement Parameters ( $\text{\AA}^2 \times 10^3$ )<sup>a</sup> for  $\text{K}_2\text{LaP}_2\text{S}_7$

	x	y	z	<i>U</i> (eq)
La(1)	0.3109(1)	0.9770(1)	0.1505(1)	12(1)
P(1)	0.0943(2)	0.5158(3)	0.1678(1)	13(1)
P(2)	0.5847(2)	1.0101(3)	0.0442(1)	12(1)
S(1)	0.2224(2)	0.9695(3)	-0.0060(1)	16(1)
S(2)	0.3046(2)	0.5650(3)	0.2172(1)	14(1)
S(3)	0.5499(2)	0.9932(3)	0.2630(1)	19(1)
S(4)	0.0802(3)	1.2754(3)	0.1082(1)	20(1)
S(5)	0.5591(3)	0.7637(3)	0.0990(1)	16(1)
S(6)	0.5305(2)	1.2489(3)	0.0963(1)	15(1)
S(7)	0.0386(3)	0.7485(3)	0.1067(1)	18(1)
K(1)	0.7606(2)	0.5110(3)	0.0094(1)	20(1)
K(2)	-0.1508(2)	1.0262(3)	0.1918(1)	29(1)

<sup>a</sup> *U*(eq) is defined as one-third of the trace of the orthogonalized  $U_{ij}$  tensor.

analogue contains 9-coordinate RE atoms.  $\text{K}_3\text{LaP}_2\text{S}_8$  contains chains of  $[\text{La}(\text{PS}_4)_2]^{3-}$  along the *x* axis that are separated by potassium cations. Along each chain lanthanum atoms are bridged by tetrahedral  $(\text{PS}_4)^{3-}$  units. Figure 4 shows that the lanthanum atoms in  $\text{K}_3\text{La}(\text{PS}_4)_2$  are coordinated by three edge-sharing  $(\text{PS}_4)^{3-}$  tetrahedra and one face-sharing  $(\text{PS}_4)^{3-}$  tetrahedron. In contrast, the lanthanum atom in  $\text{K}_3\text{La}(\text{PSe}_4)_2$  is

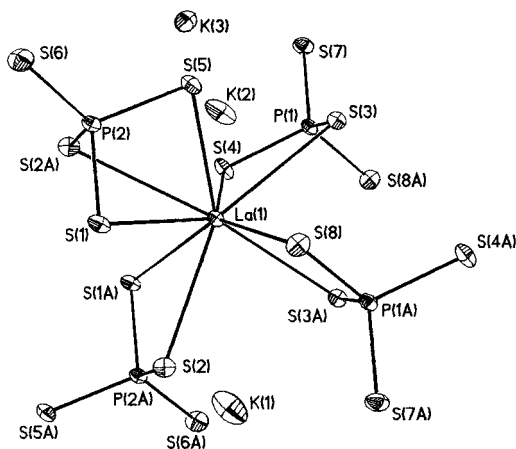


**Figure 4.** ORTEP plot of the lanthanum coordination environment in  $K_3La(PS_4)_2$ . Thermal ellipsoids plotted at the 50% probability level.

**Table 5.** Selected Bond Distances (Å) for  $K_2LaP_2S_7$

La(1)–S(3)	2.922(2)	La(1)–S(7)	2.951(3)
La(1)–S(4)	2.956(2)	La(1)–S(5)	2.974(2)
La(1)–S(6)	3.022(2)	La(1)–S(2')	3.045(2)
La(1)–S(2)	3.107(2)	La(1)–S(1)	3.145(2)
P(1)–S(4')	2.021(3)	P(1)–S(7)	2.025(3)
P(1)–S(3')	2.036(3)	P(1)–S(2)	2.058(3)
P(2)–S(1')	2.005(3)	P(2)–S(6)	2.026(3)
P(2)–S(5)	2.034(3)	P(2)–P(2')	2.195(4)

**Table 6.** Fractional Atomic Coordinates and Equivalent Isotropic Displacement Parameters ( $\text{Å}^2 \times 10^3$ )<sup>a</sup> for  $K_3La(PS_4)_2$

	x	y	z	U(eq)
La(1)	0.2269(1)	0.0137(1)	0.9697(1)	10(1)
S(1)	−0.0399(2)	0.1276(1)	0.9631(1)	14(1)
S(2)	0.0478(2)	0.0150(1)	1.2546(1)	15(1)
S(3)	0.5371(1)	0.0195(1)	0.8151(1)	13(1)
S(4)	0.3129(2)	−0.1312(1)	0.8225(1)	17(1)
S(5)	0.2090(2)	0.1201(1)	0.7189(1)	16(1)
S(6)	−0.1304(2)	0.1742(1)	0.6301(1)	20(1)
S(7)	0.5651(2)	−0.1270(1)	0.5745(1)	17(1)
S(8)	0.3379(2)	0.1587(1)	1.0919(1)	17(1)
P(1)	0.5231(1)	−0.1001(1)	0.7761(1)	11(1)
P(2)	−0.0084(2)	0.1040(1)	0.7528(1)	12(1)
K(1)	0.1194(2)	0.2039(1)	1.3761(2)	31(1)
K(2)	0.3843(2)	−0.2881(1)	0.6299(2)	37(1)
K(3)	0.2702(1)	−0.0272(1)	0.5146(1)	21(1)

<sup>a</sup>  $U(\text{eq})$  is defined as one-third of the trace of the orthogonalized  $U_{ij}$  tensor.

**Table 7.** Selected Bond Distances (Å) for  $K_3La(PS_4)_2$

La(1)–S(8)	2.9112(14)	P(1)–S(3)	2.077(2)
La(1)–S(5)	2.9929(14)	P(1)–S(4)	2.043(2)
La(1)–S(1')	3.0246(14)	P(1)–S(7)	2.003(2)
La(1)–S(2)	3.1629(14)	P(1)–S(8)	2.039(2)
La(1)–S(2')	3.317(2)	P(2)–S(1)	2.054(2)
La(1)–S(4)	2.9452(14)	P(2)–S(2)	2.062(2)
La(1)–S(3')	3.0142(14)	P(2)–S(5)	2.034(2)
La(1)–S(1)	3.119(2)	P(2)–S(6)	2.004(2)
La(1)–S(3)	3.200(2)		

coordinated by four edge-sharing  $(PS_4)^{3-}$  tetrahedra. This results from 8-coordinate lanthanum atoms versus 9-coordinate lanthanum atoms in  $K_3LaP_2S_8$  and  $K_3LaP_2S_8$ , respectively. Atomic coordinates and selected bond distances for  $K_3LaP_2S_8$  are reported in Tables 6 and 7, respectively.

A single crystal of  $K_4La_{0.67}(PS_4)_2$  or  $K_6La(PS_4)_3$  (IV) was selected, 4880 (1031 independent) reflections were collected, and an absorption correction was applied ( $R_{\text{int}} = 0.0737$ ). The structure was solved by direct methods in *Ibam* to electron density residuals of 1.154 and  $-1.064 \text{ e Å}^{-3}$ , and all atoms

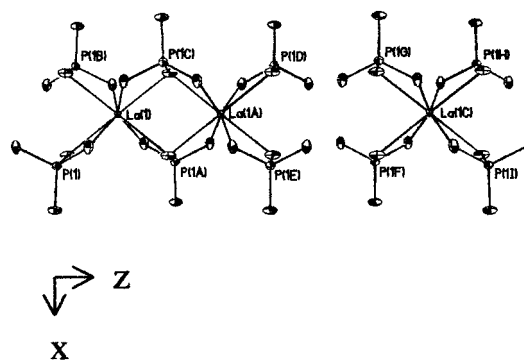


**Figure 5.** ORTEP plot of  $K_4La_{0.67}P_2S_8$ . Potassium atoms left out for clarity. Thermal ellipsoids plotted at the 50% probability level.

**Table 8.** Fractional Atomic Coordinates and Equivalent Isotropic Displacement Parameters ( $\text{Å}^2 \times 10^3$ )<sup>a</sup> for  $K_4La_{0.67}(PS_4)_2$

	x	y	z	U(eq)
La(1) <sup>b</sup>	0.0000	0.0000	0.2500	10(1)
P(1)	0.1290(1)	0.2064(2)	0.5000	15(1)
S(1)	0.0807(1)	0.2986(2)	0.3312(1)	24(1)
S(2)	0.1069(1)	0.0245(2)	0.0000	28(1)
S(3)	0.2383(1)	0.2468(2)	0.5000	27(1)
K(1)	−0.0820(1)	−0.3741(2)	0.0000	32(1)
K(2)	0.2446(1)	0.0000	0.2500	37(1)

<sup>a</sup>  $U(\text{eq})$  is defined as one-third of the trace of the orthogonalized  $U_{ij}$  tensor. <sup>b</sup> The La(1) position is only 2/3 occupied.

**Table 9.** Selected Bond Distances (Å) for  $K_4La_{0.67}(PS_4)_2$

La(1)–S(1) × 4	3.1024(14)	P(1)–S(3)	2.020(2)
La(1)–S(2) × 4	3.1302(12)	P(1)–S(1)	2.036(2)
P(1)–S(2)	2.062(3)	P(1)–S(1')	2.036(2)

were refined anisotropically with SHELXTL using full-matrix least-squares refinement on  $F^2$  for 42 variables.<sup>17</sup>  $K_4La_{0.67}(PS_4)_2$  is isostructural to  $K_4La_{0.67}(PSe_4)_2$ .<sup>12</sup> One-dimensional  $[\text{La}_{0.67}(PS_4)_2]^{4-}$  chains are found along the z axis of the unit cell. Within these chains 8-coordinate lanthanum atoms are linked together by  $(PS_4)^{3-}$  tetrahedra. As in the selenide structure, the lanthanum position is partially occupied to charge balance the formula. In a random fashion, every third lanthanum atom is “missing” along each chain. Figure 5 shows a section of these chains with La(1B) “missing”. In essence, this reduces the infinite chains into short lanthanum dimers containing two bridging  $(PS_4)^{3-}$  units and four terminal  $(PS_4)^{3-}$  units. Atomic coordinates and selected bond distances for  $K_4La_{0.67}(PS_4)_2$  are reported in Tables 8 and 9, respectively.

A single crystal of  $K_{9-x}La_{1+x/3}(PS_4)_4$  or  $K_{9-x}La_{1+x/3}P_4S_{16}$  ( $x = 0.5$ ) (V) was selected, 19212 (3880 independent) reflections were collected, and an absorption correction was applied ( $R_{\text{int}} = 0.1352$ ). The structure was solved by direct methods in *Ccca* to electron density residuals of 2.153 and  $-1.917 \text{ e Å}^{-3}$ , and all atoms were refined anisotropically with SHELXTL using full-matrix least-squares refinement on  $F^2$  for 140 variables.<sup>17</sup> The initial unit cell found by SMART [ $a = 20.23(3) \text{ Å}$ ,  $b = 9.77(1) \text{ Å}$ ,  $c = 17.52(1) \text{ Å}$ ,  $\beta = 115.84(5)^\circ$ ] matched well with the recently reported  $K_9CeP_4S_{16}$  structure.  $K_9CeP_4S_{16}$  was reported as a merohedrally twinned structure with unit cell parameters  $a = 20.242(3) \text{ Å}$ ,  $b = 9.788(1) \text{ Å}$ ,  $c = 17.524(2) \text{ Å}$ , and  $\beta = 115.36(1)^\circ$ .<sup>20</sup> However, just as in the isostructural selenide case, an acceptable structure solution could not be obtained in the  $C2/c$  space group and no evidence for twinning was found in our compound. Significant electron density was

(20) Gauthier, G.; Jobic, S.; Danaire, V.; Brec, R.; Evain, M. *Acta Crystallogr.* **2000**, C56, e117.

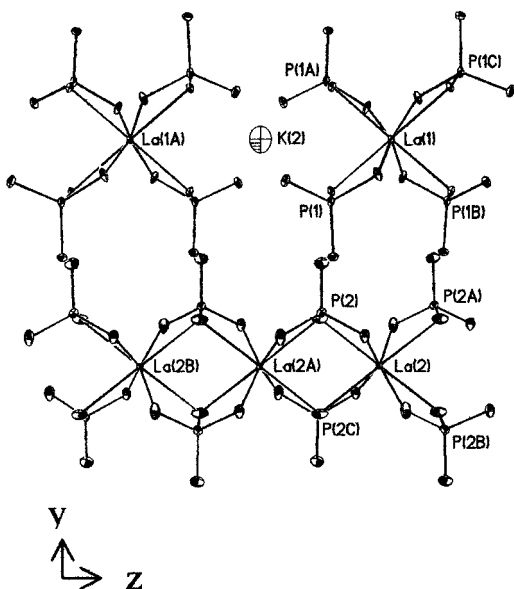


**Figure 6.** ORTEP plot of the different lanthanum coordination environments in  $K_{9-x}La_{1+x/3}(PS_4)_4$ . Thermal ellipsoids plotted at the 50% probability level.

left on one of the potassium sites, leading to a structure with a lanthanum ratio higher than 1 and a formula that could not be charge balanced. Moving to a system of higher symmetry and a larger unit cell allowed a reasonable structure solution in the orthorhombic space group  $Ccca$  with cell parameters  $a = 17.529(9)$  Å,  $b = 36.43(3)$  Å, and  $c = 9.782(4)$  Å. The structure of  $K_{9-x}La_{1+x/3}(PS_4)_4$  ( $x = 0.5$ ), shown in Figure 6, contains two different crystallographically distinct lanthanum atoms. The first lanthanum exists as isolated  ${}^0[La(PS_4)_4]^{9-}$  clusters like those observed in the  $K_9Ce(PS_4)_4$  structure. These clusters alternate with potassium atoms along the  $z$  axis of the unit cell. The second lanthanum is found in chains of lanthanum atoms linked together by  $(PS_4)^{3-}$  tetrahedra along the  $z$  axis of the unit cell. The lanthanum position along these chains is  $2/3$  occupied, just as in the  $K_4La_{0.67}(PS_4)_2$  structure. The two different lanthanum positions alternate throughout the structure.  ${}^1[La_{0.67}(PS_4)_2]^{4-}$  chains alternate with  ${}^0[La(PS_4)_4]^{9-}$  clusters along the  $x$  axis and  $y$  axis. Both lanthanum atoms exist as dodecahedra having eight La–S bonds. The average La–S bond to each lanthanum shows the difference in environments. The average La–S around each La(1) cluster is  $3.00(1)$  Å, while the average La–S bond length around each La(2) in a partially occupied chain is  $3.13(1)$  Å. Finally, the potassium atom located between La(1) isolated clusters has a rather large thermal parameter. It was refined anisotropically, but its size suggests that perhaps a partially occupied potassium atom or lanthanum exists in this position. Efforts to incorporate this into the structure solution were unsuccessful. Atomic coordinates and selected bond distances for  $K_{9-x}La_{1+x/3}(PS_4)_4$  ( $x = 0.5$ ) are reported in Tables 10 and 11, respectively.

The  $K_{9-x}La_{1+x/3}(PS_4)_4$  ( $x = 0.5$ ) formula fits well with the systematic dismantling of infinite  ${}^1[La(PS_4)_2]^{3-}$  chains in  $K_3-La(PS_4)_2$ , to shorter chains in  $K_4La_{0.67}(PS_4)_2$ , to short chains and isolated clusters in  $K_{9-x}La_{1+x/3}(PS_4)_4$ , and ending in isolated  ${}^0[La(PS_4)_4]^{9-}$  clusters in the expected  $K_9La(PS_4)_4$  structure. The  $K_{9-x}La_{1+x/3}(PS_4)_4$  and  $K_4La_{0.67}(PS_4)_2$  structures are very similar, differing only in the occupation of the rare-earth-metal sites in the crystal lattice. It is worth noting that the unit cells of these two structures are related through a transposition and doubling of both the  $a$  axis and  $b$  axis going from the  $K_4La_{0.67}$ -

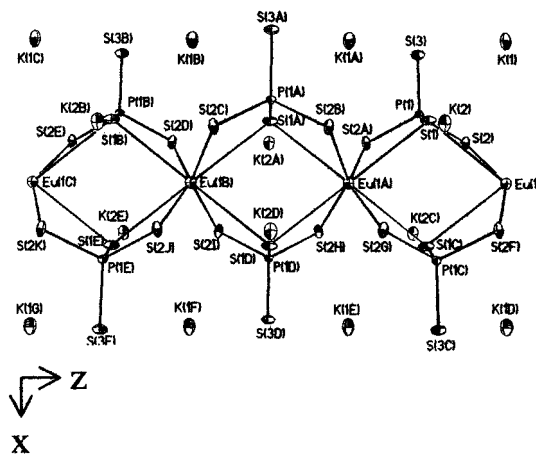


**Figure 7.** ORTEP plot of  $K_4Eu(PS_4)_2$ . Thermal ellipsoids plotted at the 50% probability level.

**Table 10.** Fractional Atomic Coordinates and Equivalent Isotropic Displacement Parameters ( $\text{Å}^2 \times 10^3$ )<sup>a</sup> for  $K_{9-x}La_{1+x/3}(PS_4)_4$  ( $x = 0.5$ )

	x	y	z	$U(\text{eq})$
La(1)	0.0000	0.2500	0.7500	7(1)
La(2) <sup>b</sup>	0.2500	0.0000	0.7460(1)	7(1)
S(1)	0.0119(2)	0.1960(1)	0.5215(3)	9(1)
S(2)	0.1474(2)	0.2124(1)	0.8226(3)	15(1)
S(3)	-0.1531(2)	0.2064(4)	0.3405(4)	16(1)
S(4)	-0.1240(2)	0.1307(1)	0.5179(4)	16(1)
S(5)	0.0999(2)	0.0407(1)	0.6644(4)	21(1)
S(6)	0.2392(3)	0.0535(1)	0.9959(4)	28(1)
S(7)	0.4005(2)	0.0400(1)	0.8284(4)	26(1)
S(8)	0.1260(3)	0.1192(1)	0.4944(3)	24(1)
K(1)	0.1869(2)	0.2912(1)	1.0166(3)	22(1)
K(2)	0.0000	0.2500	0.2500	93(4)
K(3)	0.0000	0.1251(1)	0.7500	24(1)
K(4)	0.4364(2)	-0.0410(1)	0.9995(3)	26(1)
K(5)	-0.2463(2)	0.1218(1)	0.2632(3)	27(1)
K(6)	0.0000	0.1321(1)	0.2500	31(1)
P(1)	-0.1042(2)	0.1856(1)	0.5107(3)	11(1)
P(2)	0.1466(3)	0.0647(1)	0.4954(3)	13(1)

<sup>a</sup>  $U(\text{eq})$  is defined as one-third of the trace of the orthogonalized  $U_{ij}$  tensor. <sup>b</sup> The La(2) position is only  $2/3$  occupied.

**Table 11.** Selected Bond Distances (Å) for  $K_{9-x}La_{1+x/3}(PS_4)_4$  ( $x = 0.5$ )

La(1)–S(1) × 4	2.983(3)	P(1)–S(2)	2.047(5)
La(1)–S(2) × 4	3.009(4)	P(1)–S(3)	2.021(5)
La(2)–S(7) × 2	3.119(4)	P(1)–S(4)	2.030(6)
La(2)–S(5) × 2	3.123(4)	P(2)–S(5)	2.043(5)
La(2)–S(6) × 2	3.131(4)	P(2)–S(6)	2.044(7)
La(2)–S(6) × 2	3.134(4)	P(2)–S(7)	2.040(5)
P(1)–S(1)	2.073(5)	P(2)–S(8)	2.018(7)

$(PS_4)_2$  to the  $K_{9-x}La_{1+x/3}(PS_4)_4$  structure. Perhaps a smaller rare-earth-metal cation and larger alkali-metal cation would give the  $K_9Ce(PS_4)_4$  structure type with its isolated clusters.

A single crystal of  $K_4Eu(PS_4)_2$  or  $K_4EuP_2S_8$  (VI) was selected, 4965 (1020 independent) reflections were collected, and an absorption correction was applied ( $R_{\text{int}} = 0.0893$ ). The structure was solved by direct methods in *Ibam* to electron density residuals of 1.340 and  $-1.442 \text{ e Å}^{-3}$ , and all atoms were refined anisotropically with SHELXTL using full-matrix least-squares refinement on  $F^2$  for 42 variables.<sup>17</sup>  $K_4EuP_2S_8$  is isostructural to  $K_4Eu(PSe_4)_2$ .<sup>21</sup> Figure 7 shows that chains of  $[Eu(PS_4)_2]^{4-}$  propagate along the  $z$  axis and are separated by potassium

(21) Chondroudis, K.; McCarthy, T. J.; Kanatzidis, M. G. *Inorg. Chem.* **1996**, *35*, 840–844.

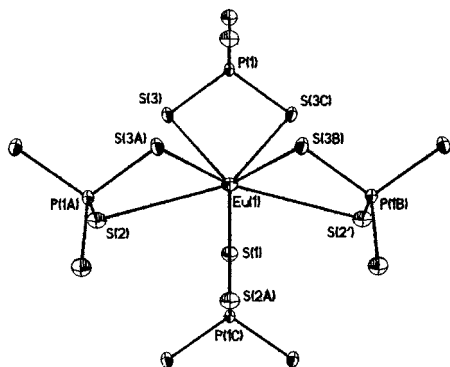


**Figure 8.** ORTEP plot of  $\text{K}_4\text{Eu}(\text{PS}_4)_2$ . Thermal ellipsoids plotted at the 50% probability level. Potassium atoms left out for clarity.

**Table 12.** Fractional Atomic Coordinates and Equivalent Isotropic Displacement Parameters ( $\text{\AA}^2 \times 10^3$ )<sup>a</sup> for  $\text{K}_4\text{Eu}(\text{PS}_4)_2$

	x	y	z	$U(\text{eq})$
Eu(1)	0.5000	0.0000	0.2500	12(1)
P(1)	0.3714(2)	0.2053(3)	0.0000	6(1)
S(1)	0.3941(2)	0.0238(3)	0.5000	13(1)
S(2)	0.4194(1)	0.2982(3)	0.1695(2)	13(1)
S(3)	0.2615(2)	0.2463(4)	0.0000	13(1)
K(1)	0.2575(2)	0.0000	0.2500	20(1)
K(2)	0.5833(2)	-0.3763(3)	0.5000	15(1)

<sup>a</sup>  $U(\text{eq})$  is defined as one-third of the trace of the orthogonalized  $U_{ij}$  tensor.

**Table 13.** Selected Bond Distances ( $\text{\AA}$ ) for  $\text{K}_4\text{Eu}(\text{PS}_4)_2$

Eu(1)–S(2')	3.113(5)	Eu(1)–S(2')	3.114(5)
Eu(1)–S(2)	3.114(5)	Eu(1)–S(2')	3.114(5)
Eu(1)–S(1')	3.119(4)	Eu(1)–S(1')	3.119(4)
Eu(1)–S(1)	3.119(4)	Eu(1)–S(1')	3.119(4)
P(1)–S(2)	2.041(3)	P(1)–S(2')	2.041(3)
P(1)–S(3)	2.042(7)	P(1)–S(1')	2.062(5)

cations. Dodecahedral europium atoms are bridged by  $(\text{PS}_4)^{3-}$  tetrahedra in an edge-sharing manner. The average Eu–S bond distance is 3.12(1)  $\text{\AA}$ . Atomic coordinates and selected bond distances for  $\text{K}_4\text{EuP}_2\text{S}_8$  are reported in Tables 12 and 13, respectively.

A single crystal of  $\text{KEuPS}_4$  (**VII**) was selected, 4521(977 independent) reflections were collected, and an absorption correction was applied ( $R_{\text{int}} = 0.0581$ ). The structure was solved by direct methods in  $Pnma$  to electron density residuals of 1.047 and  $-1.209 \text{ e \AA}^{-3}$ , and all atoms were refined anisotropically with SHELXTL using full-matrix least-squares refinement on  $F^2$  for 40 variables.<sup>17</sup>  $\text{KEuPS}_4$  is isostructural to  $\text{KEuPSe}_4$ <sup>12</sup> and isotypic to  $\text{CsPbPSe}_4$ .<sup>21</sup> It is a two-dimensional structure with  ${}_{\infty}^2[\text{EuPS}_4]^-$  layers in the  $yz$  plane separated by potassium cations. 8-Coordinate bicapped trigonal prism europium atoms are linked into a layer by  $(\text{PS}_4)^{3-}$  tetrahedra. Each  $(\text{PS}_4)^{3-}$  tetrahedron is coordinated to four different europium atoms. Just as in  $\text{KEuPSe}_4$ , the europium atoms in  $\text{KEuPS}_4$  have two Eu–S bonds that are longer than the other six Eu–S bonds. The two longer bonds have a Eu–S bond distance of 3.4232(7)  $\text{\AA}$ , while the shorter Eu–S bonds range from 2.966(2) to 3.086(2)  $\text{\AA}$ . In Figure 8 these longer bonds are between Eu(1) and S(2), while the shorter bonds are to S(1), S(2A), and S(3). Eu(II) sits in a trigonal prism of sulfur atoms and is capped on each side of the prism by longer Eu–S bonds. This type of bonding has been observed before in  $\text{Eu}_2\text{BiSi}_4$ <sup>22</sup> and  $\text{Eu}_3\text{Sb}_4\text{S}_9$ .<sup>23</sup> Atomic coordi-

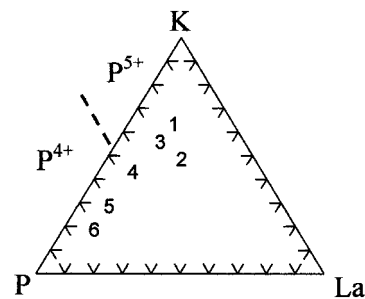


**Figure 9.** La–P–K ternary phase diagram. Numbers represent the ratio of La–P–K in a particular reaction mixture.

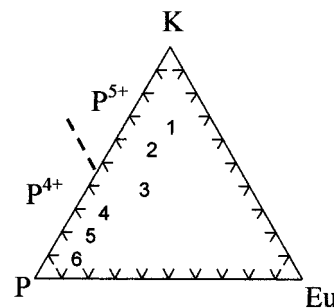


**Figure 10.** Eu–P–K ternary phase diagram. Numbers represent the ratio of Eu–P–K in a particular reaction mixture.

**Table 14.** Fractional Atomic Coordinates and Equivalent Isotropic Displacement Parameters ( $\text{\AA}^2 \times 10^3$ )<sup>a</sup> for  $\text{KEuPS}_4$

	x	y	z	$U(\text{eq})$
Eu(1)	0.4780(1)	0.2500	0.2919(1)	14(1)
P(1)	0.4020(1)	0.2500	0.7786(4)	10(1)
K(1)	0.2117(1)	0.2500	0.4815(4)	24(1)
S(1)	0.3324(1)	0.2500	0.0338(4)	17(1)
S(2)	0.4785(1)	-0.2500	0.1562(4)	16(1)
S(3)	0.3786(1)	0.0027(2)	0.6013(3)	14(1)

<sup>a</sup>  $U(\text{eq})$  is defined as one-third of the trace of the orthogonalized  $U_{ij}$  tensor.

**Table 15.** Selected Bond Distances ( $\text{\AA}$ ) for  $\text{KEuPS}_4$

Eu(1)–S(1)	2.966(2)	Eu(1)–S(2')	3.009(2)
Eu(1)–S(3')	3.012(2)	Eu(1)–S(3')	3.012(2)
Eu(1)–S(3')	3.086(2)	Eu(1)–S(3)	3.086(2)
Eu(1)–S(2)	3.4232(7)	Eu(1)–S(2')	3.4232(7)
P(1)–S(1')	2.032(3)	P(1)–S(3')	2.041(2)
P(1)–S(3)	2.041(2)	P(1)–S(2')	2.050(3)

nates and selected bond distances for  $\text{KEuPS}_4$  are reported in Tables 14 and 15, respectively.

**Phase Diagrams.** Quasi-quaternary Gibbs-type phase diagrams were constructed by plotting the reaction conditions that produced the crystal structures described above. Both the La–P–K–S and Eu–P–K–S phase diagrams are similar to their selenium counterparts. All reactions represented in Figures 9 and 10 were done under a relative thermodynamic equilibrium isotherm of 725  $^\circ\text{C}$  and were isometric in sulfur with some expected variation. In these phase diagrams, numbers represent reactions wherein various ratios of  $\text{K}/(\text{K} + \text{P} + \text{RE})$ ,  $\text{P}/(\text{K} + \text{P} + \text{RE})$ , and  $\text{RE}/(\text{K} + \text{P} + \text{RE})$  were used. Tables 16 and 17 list these ratios for each phase diagram point. In this way, the RE–P–K phase diagrams can be thought of as an isometric sulfur slice through a quaternary RE–P–K–S phase diagram.

**La–P–K System.** The isothermal La–P–K phase diagram in Figure 9 contains five different crystalline products:  $\text{KLaP}_2\text{S}_6$

(22) Lemoine, P. P.; Carre, D.; Guittard, M. *Acta Crystallogr.* **1982**, *B38*, 727–729.

(23) Lemoine, P. P.; Carre, D.; Guittard, M. *Acta Crystallogr.* **1981**, *B37*, 1281–1284.

**Table 16.** Reactant Ratios Represented in Figure 9

phase diagram point(s)	K/(K + P + La)	P/(K + P + La)	La/(K + P + La)	reaction product
1	0.65	0.2	0.15	$K_3PS_4$
2	0.5	0.25	0.25	$K_4La_{0.67}(PS_4)_2$
3	0.5714	0.2857	0.1429	$K_3La(PS_4)_2$
4	0.4444	0.4444	0.1111	$K_2La(P_2S_6)_{1/2}(PS_4)$
5	0.3	0.6	0.1	
6	0.2	0.7	0.1	$KLAP_2S_6$

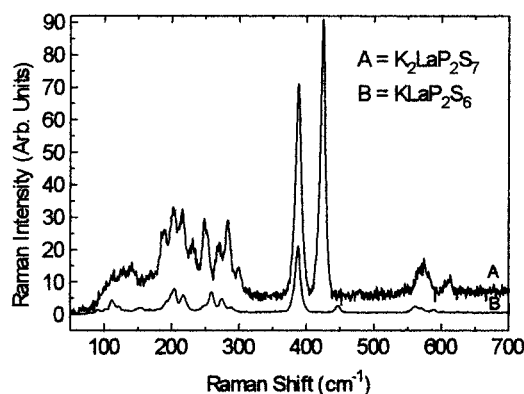
**Table 17.** Reactant Ratios Represented in Figure 10

phase diagram point	K/(K + P + Eu)	P/(K + P + Eu)	Eu/(K + P + Eu)	reaction product
1	0.6667	0.1667	0.1667	$K_4Eu(PS_4)_2$
2	0.5714	0.2857	0.1429	
3	0.4	0.4	0.2	$KEuPS_4$
4	0.3	0.6	0.1	$Eu_2P_2S_6$
5	0.2	0.7	0.1	
6	0.1	0.8	0.1	

(I),  $K_2LaP_2S_7$  (II),  $K_3La(PS_4)_2$  (III),  $K_4La_{0.67}(PS_4)_2$  (IV), and  $K_{9-x}La_{1+x/3}(PS_4)_4$  ( $x = 0.5$ ) (V). At point 1, the point with the highest potassium molar ratio and lowest phosphorus and lanthanum molar ratios, only the ternary compound  $K_3PS_4$ <sup>24</sup> is found as a crystalline product. This indicates the edge of where we will find quaternary compounds in this phase diagram. Decreasing the potassium molar ratio while simultaneously increasing the phosphorus molar ratio changes the observed product. Compound IV is observed at point 2, and compound III is observed at point 3. Compound V has not been observed as single crystals at 725 °C as it was only found in reactions below 550 °C. We would expect it to be found between points 1 and 3 on the phase diagram. Up to point 3 only P<sup>V</sup> was found in the crystalline products as  $(PS_4)^{3-}$  units. Increasing the phosphorus molar ratio to 45% finally brings us to the area of the phase diagram where P<sup>IV</sup> is found.  $K_2LaP_2S_7$  was observed at points 4 and 5 and contains both P<sup>V</sup> and P<sup>IV</sup>. Finally, at point 6, only P<sup>IV</sup> was observed in the  $KLAP_2S_6$  structure.

**Eu–P–K System.** The Eu–P–K phase diagram in Figure 10 contains only three different crystalline products.  $K_4Eu(PS_4)_2$  and  $KEuPS_4$  have been reported here. The third compound,  $Eu_2P_2S_6$ , observed as a crystalline product, was previously reported.<sup>25</sup>  $K_4Eu(PS_4)_2$  was the crystalline product observed at the highest potassium molar ratios and lowest phosphorus molar ratios (points 1 and 2). Decreasing the potassium molar ratio while increasing the phosphorus molar ratio led to the  $KEuPS_4$  compound at point 3. Both  $K_4Eu(PS_4)_2$  and  $KEuPS_4$  contain P<sup>V</sup>. P<sup>IV</sup> was not found until very high phosphorus molar ratios at points 4–6 in the  $Eu_2P_2S_6$  compound. As in the selenide case, a quaternary compound was not found containing both P<sup>V</sup> and P<sup>IV</sup>.

The major difference observed between the sulfur and selenium phase diagrams is the greater oxidizing power of the  $S^0/S^{2-}$  flux compared to the  $Se^0/Se^{2-}$  flux. Because sulfur is a better oxidizing agent, we see phosphorus in its highest oxidation state, P<sup>V</sup>, in a larger area of the phase diagram. For example, in the selenide version of the europium phase diagram, P<sup>IV</sup> is observed for the first time at approximately a 40% mole ratio of phosphorus. In the sulfur version of the phase diagram, P<sup>IV</sup> is not observed until ~60% mole ratio of phosphorus. An additional effect of the oxidizing power of sulfur versus selenium

**Figure 11.** Raman spectra of  $KLAP_2S_6$  and  $K_2La(P_2S_6)_{1/2}(PS_4)$ .**Table 18.** *l–o* Values, Predicted Formulas, and Reported Structures for  $(A_4P_2S_6)_l(A_3PS_4)_m(La_4(P_2S_6)_3)_n(LaPS_4)_o$  and  $(A_4P_2S_6)_l(A_3PS_4)_m(Eu_2(P_2S_6))_n[(Eu_3(PS_4)_2)_o]$ 

l	m	n	o	predicted formula	reported structure
$(A_4P_2S_6)_l(A_3PS_4)_m(La_4(P_2S_6)_3)_n(LaPS_4)_o$					
0	1	0	0	$A_3PS_4$	$K_3PS_4$
1	0	0	0	$A_4P_2S_6$	$K_4P_2S_6$
0	0	1	0	$La_4(P_2S_6)_3$	
0	0	0	1	$LaPS_4$	
1	0	1	0	$A_4La_4(P_2S_6)_4$	$KLAP_2S_6$
1	0	0	2	$A_4La_2(P_2S_6)_2(PS_4)_2$	$K_2La(P_2S_6)_{1/2}(PS_4)$
0	1	0	1	$A_3La(PS_4)_2$	$K_3La(PS_4)_2$
0	2	0	1	$A_6La(PS_4)_3$	$K_4La_{0.67}(PS_4)_2$
0	3	0	1	$A_9La(PS_4)_4$	$K_{9-x}La_{1+x/3}(PS_4)_4$
$(A_4P_2S_6)_l(A_3PS_4)_m(Eu_2(P_2S_6))_n[(Eu_3(PS_4)_2)_o]$					
0	0	1	0	$Eu_2P_2S_6$	$Eu_2P_2S_6$ <sup>25</sup>
0	0	0	1	$Eu_3(PS_4)_2$	
1	0	1	0	$A_4Eu_2(P_2S_6)_2 \equiv A_2EuP_2S_6$	
0	1	0	1	$A_3Eu_3(PS_4)_3$	$KEuPS_4$
0	4	0	1	$A_{12}Eu_3(PS_4)_6$	$K_4Eu(PS_4)_2$
0	7	0	1	$A_{21}Eu_3(PS_4)_9 \equiv A_7Eu(PS_4)_3$	
0	10	0	1	$A_{30}Eu_3(PS_4)_{12} \equiv A_{10}Eu(PS_4)_4$	

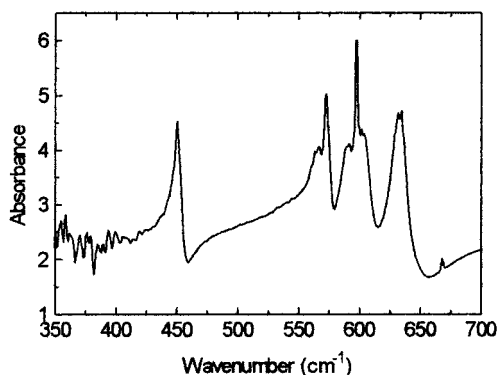
is that P<sup>III</sup> was not found in the sulfur phase diagrams. In both diagrams P<sup>IV</sup> extends to the edge of the phase space. Perhaps ternary or quaternary structures with P<sup>III</sup> can be found in a different isometric “slice” of the quaternary phase diagram.<sup>26</sup>

The same formulas used in the previous paper can be used to describe the dismantling of rare-earth-metal thiophosphates into two- and one-dimensional structures by the addition of  $(P_2S_6)^{4-}$  and  $(PS_4)^{3-}$  units. A similar set of target compounds is listed in Table 18.

**Vibrational and Electronic Spectroscopy.** Figure 11 shows the Raman spectra for  $KLAP_2S_6$  and  $K_2La(P_2S_6)_{1/2}(PS_4)$ .  $KLAP_2S_6$  contains vibrations expected for the  $(P_2S_6)^{4-}$  unit, while  $K_2La(P_2S_6)_{1/2}(PS_4)$  contains vibrations for both the  $(P_2S_6)^{4-}$  unit and the  $(PS_4)^{3-}$  unit. The peak at 387  $cm^{-1}$ , observed in both spectra, is assigned to the  $A_{1g}$  symmetric stretch of the  $(P_2S_6)^{4-}$  unit. The peak at 424  $cm^{-1}$ , observed only in the  $K_2La(P_2S_6)_{1/2}(PS_4)$  spectra, is assigned to the  $A_1$  symmetric stretch of the tetrahedral  $(PS_4)^{3-}$  unit. Vibrations above 500  $cm^{-1}$  in both spectra are asymmetric stretching vibrations from  $(P_2S_6)^{4-}$  and/or  $(PS_4)^{3-}$  units, and peaks below 350  $cm^{-1}$  are bending vibrations. The peak at 447  $cm^{-1}$  is found only in the Raman spectrum of  $KLAP_2S_6$ . It is assigned to an  $A_{2u}$  vibrational mode of the  $(P_2S_6)^{4-}$  unit. This peak is normally only IR active, but in  $KLAP_2S_6$  it is observed in both the Raman and IR spectra. The IR absorbance spectrum for  $KLAP_2S_6$ , shown in Figure 12,

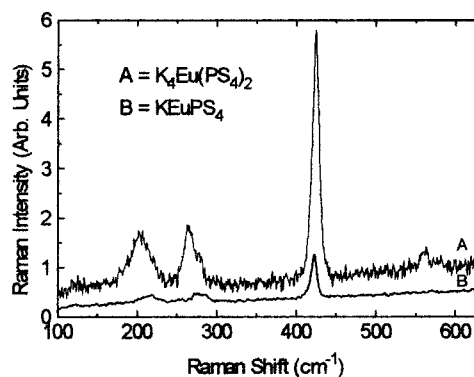
(24) Schafer, H.; Schafer, G.; Weiss, A. *Z. Naturforsch.* **1965**, *20b*, 811.(25) Brockner, W.; Becker, R. *Z. Naturforsch.* **1987**, *42a*, 511–512.

(26) Evenson, C. R.; Dorhout, P. K. Unpublished results.

Figure 12. IR spectrum of KLaP<sub>2</sub>S<sub>6</sub>.Table 19. Raman Peaks (cm<sup>-1</sup>) Found in KLaP<sub>2</sub>S<sub>6</sub>, K<sub>2</sub>FeP<sub>2</sub>S<sub>6</sub>,<sup>27</sup> and K<sub>2</sub>LaP<sub>2</sub>S<sub>7</sub>

KLaP <sub>2</sub> S <sub>6</sub>	K <sub>2</sub> FeP <sub>2</sub> S <sub>6</sub>	K <sub>2</sub> LaP <sub>2</sub> S <sub>7</sub>	KLaP <sub>2</sub> S <sub>6</sub>	K <sub>2</sub> FeP <sub>2</sub> S <sub>6</sub>	K <sub>2</sub> LaP <sub>2</sub> S <sub>7</sub>
90			288	280	283
111		114			300
		140		378	
153		156	387 (A <sub>1g</sub> )	391	387 (A <sub>1g</sub> )
	183	188			424 (A <sub>1</sub> )
204		202	447 (A <sub>2u</sub> ) <sup>a</sup>	453 <sup>b</sup>	
217		215	561	565	570
	228	231	589	585	574
259	245	248			613
275		270			

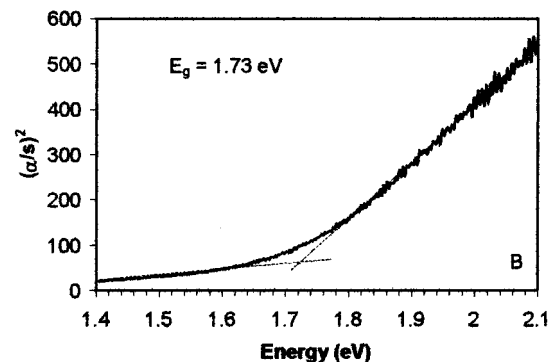
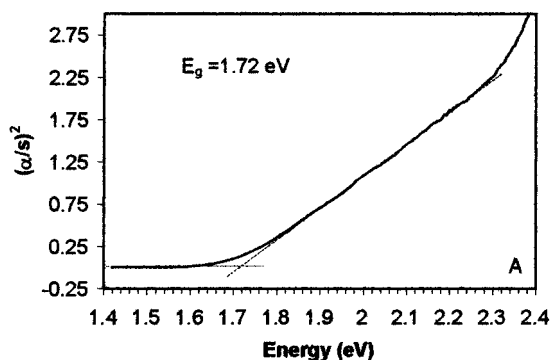
<sup>a</sup> Observed in Raman spectrum. <sup>b</sup> Observed in IR spectrum.

Figure 13. Raman spectra of K<sub>4</sub>Eu(PS<sub>4</sub>)<sub>2</sub> and KEuPS<sub>4</sub>.

clearly shows the same peak at 450 cm<sup>-1</sup>. There is no inversion center located between the two phosphorus atoms in KLaP<sub>2</sub>S<sub>6</sub>. Because of this, the (P<sub>2</sub>S<sub>6</sub>)<sup>4-</sup> unit does not have idealized D<sub>3d</sub> symmetry, which probably allows the A<sub>2u</sub> peak to be observed in the Raman spectrum. In K<sub>2</sub>La(P<sub>2</sub>S<sub>6</sub>)<sub>1/2</sub>(PS<sub>4</sub>) there is an inversion center located between the phosphorus atoms in the (P<sub>2</sub>S<sub>6</sub>)<sup>4-</sup> units, and we do not see the peak at 447 cm<sup>-1</sup> in its Raman spectrum. Table 19 lists the Raman peaks found for KLaP<sub>2</sub>S<sub>6</sub> and K<sub>2</sub>La(P<sub>2</sub>S<sub>6</sub>)<sub>1/2</sub>(PS<sub>4</sub>). Both the Raman and IR assignments for the (P<sub>2</sub>S<sub>6</sub>)<sup>4-</sup> unit match well with those values reported for K<sub>2</sub>Fe(P<sub>2</sub>S<sub>6</sub>).<sup>27</sup>

As in the selenide structures, the K<sub>3</sub>La(PS<sub>4</sub>)<sub>2</sub>, K<sub>4</sub>La<sub>0.67</sub>(PS<sub>4</sub>)<sub>2</sub>, and K<sub>9-x</sub>La<sub>1+x/3</sub>(PS<sub>4</sub>)<sub>4</sub> compounds all show the four Raman peaks expected for the (PS<sub>4</sub>)<sup>3-</sup> unit.

Figure 13 shows the Raman spectra of K<sub>4</sub>Eu(PS<sub>4</sub>)<sub>2</sub> and KEuPS<sub>4</sub>. Both spectra show the four vibrational modes expected for the (PS<sub>4</sub>)<sup>3-</sup> unit.<sup>28</sup> The large peak at 424 cm<sup>-1</sup> is assigned

Figure 14. Optical band gap spectra for (A) K<sub>4</sub>Eu(PS<sub>4</sub>)<sub>2</sub> and (B) KEuPS<sub>4</sub>.

to the symmetric stretch, and the peak at ~570 cm<sup>-1</sup> corresponds to the asymmetric stretch. The two peaks below 300 cm<sup>-1</sup> correspond to bending vibrations.

All four potassium lanthanum phosphorus sulfides are found as clear crystals with optical band gaps above 3.5 eV. Figure 14 shows the optical band gaps of K<sub>4</sub>Eu(PS<sub>4</sub>)<sub>2</sub> and KEuPS<sub>4</sub>. Both were found as clear, brown crystals with optical band gaps of 1.72 and 1.73 eV, respectively.

## Conclusions

We have extended the use of ternary phase diagrams for the synthesis of new rare-earth-metal polychalcophosphates to the sulfur system. Compounds I–VII were synthesized using the reactive flux method and characterized using single-crystal X-ray diffraction, Raman and IR spectroscopy, and optical band gap analysis. Plotting the reactive flux conditions in a ternary phase diagram allows a visual understanding of the different molar ratios necessary for the synthesis of different products. These phase diagrams, constructed under the appropriate reaction conditions, offer a useful tool for understanding the conditions needed to rationally approach the synthesis of new compounds with desirable properties.

**Acknowledgment.** This work was supported by the National Science Foundation (Grant CHE-9625378) and an NSF-MRI Instrumentation Grant.

**Supporting Information Available:** Tables of additional crystallographic details, all bond distances and angles, and anisotropic thermal parameters. This material is available free of charge via the Internet at <http://pubs.acs.org>.

IC000596R

(27) Carrillo-Cabrera, W.; Sabmannshausen, J.; von Schnering, H. G.; Menzel, F.; Brockner, W. *Z. Anorg. Allg. Chem.* **1994**, *620*, 489–494.

(28) Muller, A.; Mohan, N.; Cristophlienck, P.; Tossidis, I.; Drager, M. *Spectrochim. Acta* **1973**, *29A*, 1345.